Frequency-Swept Microwave Imaging of Dielectric Objects

TAH-HSIUNG CHU, MEMBER, IEEE AND NABIL H. FARHAT, FELLOW, IEEE

Abstract—**In this paper, analytical and experimental studies of frequency-swept microwave imaging of a nondispersive dielectric object satisfying the Born approximation are presented. The retrieved images shown from experimental data measured in the frequency range 6–17 GHz are free of the speckle noise that plagues conventional coherent imaging system. The results demonstrate that the microwave imaging system described here has potential as a cost-effective tool in nondestructive evaluation of dielectric objects.**

I. Introduction

THE ABILITY OF microwaves to propagate through optically opaque dielectrics makes microwave holography useful for remote sensing and nondestructive evaluation (NDE) of dielectric structures. This is accomplished by recording and analyzing the wave field scattered by coherently illuminated dielectric structures. The use of frequency diversity has been demonstrated to be an effective means for accessing the 3-D Fourier space of a scattering body and for the retrieval of tomographic or projective images of the body [1]–[3] based on the projection-slice theorem [4]. Automated and efficient data acquisition is achieved by combining angular and spectral diversity.

In this paper, we make use of the fact that the normalized scattered far field of a dielectric object, under the first-order Born approximation, is related to the Fourier transform of the derivative of the dielectric constant of the test object [5]. Therefore, based upon the projection-slice theorem, either direct Fourier inversion or a filtered-back-projection algorithm can be applied to obtain a projective or tomographic image of dielectric bodies from the accessed spectral (or Fourier space) data. Experimental results of projection imagery of two concentric plexiglass cylinders viewed at different orientations demonstrate the utility of the methods in imaging penetrable objects and visualizing the internal structure in nondestructive evaluation.

II. Theoretical Considerations

In this section, we will present the principle of bistatic microwave imaging of a nondispersive dielectric object using the frequency diversity technique. The dielectric object (see Fig. 1) possessing a relative dielectric constant $\epsilon_r(\bar{r}')$ and situated in a lossless, homogeneous medium, here assumed to be air ($\epsilon_r = 1$), is illuminated by a plane wave $\Psi_i(k, \bar{r})$ traveling in the direction of the unit vector $\hat{i}_k$, where

$$\Psi_i(k, \bar{r}) = e^{j\bar{k}_i \cdot \bar{r}} \tag{1}$$

$\bar{k}_i = k\hat{i}_k$ being the wave vector of the incident wave, $\bar{r}$ and $\bar{r}'$ are position vectors, and $\exp(-j\omega t)$ is implied. The total field $\Psi(k, \bar{r})$ at the observation or field point $O(\bar{r})$ satisfies the scalar Helmholtz equation [5]

$$\left[\nabla^2 + k^2\epsilon_r(\bar{r})\right]\Psi(k, \bar{r}) = 0 \tag{2}$$

where $\Psi(k, \bar{r}) = \Psi_i(k, \bar{r}) + \Psi_s(k, \bar{r})$, with $\Psi_s(k, \bar{r})$ being the scattered wave field, and

$$\epsilon_r(\bar{r}) = \begin{cases} \epsilon_r(\bar{r}') & \bar{r} \in v' \\ 1 & \bar{r} \notin \epsilon'. \end{cases} \tag{3}$$

Equation (2) can then be written as

$$\left[\nabla^2 + k^2\right]\Psi_s(k, \bar{r}) = -k^2\left[\epsilon_r(\bar{r}) - 1\right]\Psi(k, \bar{r}). \tag{4}$$

Assuming that the dielectric object is weakly scattering, i.e., $\epsilon_r(\bar{r}') = 1 + \Delta\epsilon_r(\bar{r}')$ (and hence the first-order Born approximation holds), (4) can then be expressed as

$$\left[\nabla^2 + k^2\right]\Psi_s(k, \bar{r}) = -k^2\Delta\epsilon_r(\bar{r})\Psi_i(k, \bar{r}) \tag{5}$$

where

$$\Delta\epsilon_r(\bar{r}) = \begin{cases} \Delta\epsilon_r(\bar{r}') & \bar{r} \in v' \\ 0 & \bar{r} \notin v' \end{cases} \tag{6}$$

and $-k^2\Delta\epsilon_r(r)$ is known as the scattering potential [5] of the dielectric body.

The solution of (5) for the scattered field for the case of plane wave illumination and under the first-order Born approximation can be shown, referring to Fig. 1, to be [5]

$$\Psi_s(k, \bar{r}) = -k^2\int G(\bar{r} - \bar{r}')\,\Delta\epsilon_r(\bar{r}')\,\Psi_i(k, \bar{r}')\,dv' \tag{7}$$

where dv' designates an element of volume of the object, and

$$G(\bar{r} - \bar{r}') = \frac{e^{jk|\bar{r} - \bar{r}'|}}{4\pi|\bar{r} - \bar{r}'|} = \frac{e^{jkR}}{4\pi R} \tag{8}$$

is the Green's function. The integration in (7) is taken over all space, because $\Delta\epsilon_r(\bar{r})$ is zero outside the dielectric object.

Manuscript received May 23, 1987; revised September 16, 1987.

T.-H. Chu is with the Electrical Engineering Department, National Taiwan University, Taipei, Taiwan, Republic of China

N. H. Farhat is with the Electrical Engineering Department, University of Pennsylvania, Philadelphia, PA 19104.

IEEE Log Number 8718370.

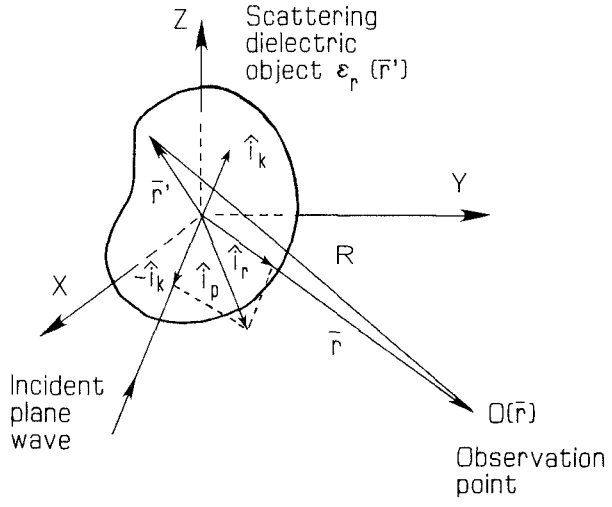

Fig. 1. Frequency-swept microwave imaging geometry.

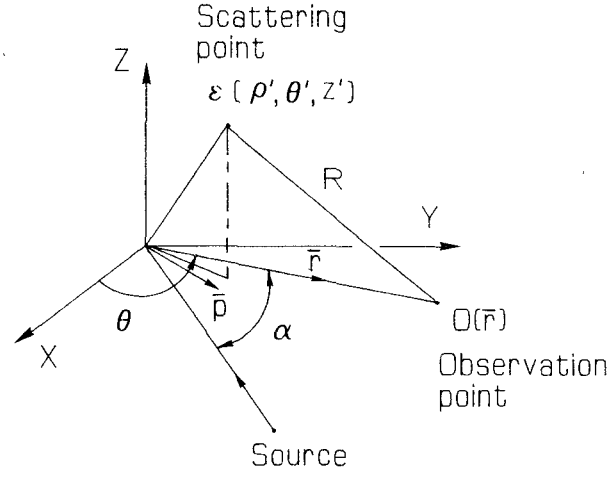

Fig. 2. Geometry used in swept frequency microwave imaging experiment.

A frequency-swept microwave imaging system can be implemented as shown in Fig. 2, where the transmitter and coherent receiver are located in the $x-y$ plane and the dielectric object with scattering point (secondary source point) position (ρ', θ', z') is rotated in the θ direction about the z axis in order to be viewed at different azimuthal aspect angles. The total scattered field is then

$$\Psi_s(k, \bar{r}) = \Psi_s(k, r, \theta) = \frac{-k^2}{4\pi} \iiint \frac{e^{jkR}}{R} \Delta\epsilon_r(\rho', \theta', z')\, e^{j\bar{k}_i \cdot \bar{r}'}\, dv'. \quad (9)$$

Since we have assumed the observation point is in the far field, the distance R from the scatterer to the observation point O($\bar{r}$) can be simplified as

$$R = |\bar{r} - \bar{r}'| \cong r - \hat{i}_r \cdot \bar{r}' + r'^2/2r. \quad (10)$$

The last term in (10) can be neglected if the observation point is in the far field, i.e.,

$$r > \frac{\pi r'^2}{\text{wavelength}}. \quad (11)$$

Therefore, (9) becomes

$$\Psi_s(k, r, \theta) = \frac{-k^2 e^{jkr}}{4\pi r} \iiint \Delta\epsilon_r(\rho', \theta', z')\, e^{jk(\hat{i}_k - \hat{i}_r)\cdot \bar{r}'} \rho'\, d\rho'\, d\theta'\, dz' = \frac{-k^2 e^{jkr}}{4\pi r} \iiint \Delta\epsilon_r(\rho', \theta', z')\, e^{-j\bar{p}\cdot\bar{r}'} \rho'\, d\rho'\, d\theta'\, dz'. \quad (12)$$

Since $\bar{r}'$ as seen from Fig. 2 is a function of ρ', θ', and z', the integral in (12) is recognized as the 3-D Fourier transform of the dielectric constant difference, where

$$\bar{p} = \bar{k}_r - \bar{k}_i = k(\hat{i}_r - \hat{i}_k) = 2k\cos(\alpha/2)\hat{i}_p = p\hat{i}_p = p\left[\cos(\theta - \alpha/2)\hat{i}_x + \sin(\theta - \alpha/2)\hat{i}_y\right]$$

is the position vector in the Fourier space $\Gamma(\bar{p})$, the normalized scattered wave field, defined as

$$\Gamma(\bar{p}) = \Gamma(p, \theta) = \frac{\Psi_s(k, r, \theta)}{\Psi_{\text{ref}}(k, r)}. \quad (13)$$

Here $\Psi_{\text{ref}}(k, r) = (jk/4\pi r)\exp(jkr)$ is the scattered wave field of a perfectly conducting cylinder which is used as a reference object for range-phase term removal. The reference cylinder is positioned such that its axis is in the z direction and its front surface coincides with the axis of the turntable described in [2] and [3].

The quantity $\Gamma(p, \theta)$ is a two-dimensional slice in the 3-D Fourier space of the scattering dielectric object, which, according to (12) and (13), is given by

$$\Gamma(p, \theta) = jk \iiint \Delta\epsilon_r(\rho', \theta', z')\, e^{-j\bar{p}\cdot\bar{r}'} \rho'\, d\rho'\, d\theta'\, dz' = jk \iiint \left[\int \Delta\epsilon_r(\rho', \theta', z')\, dz'\right] e^{-j\bar{p}\cdot\bar{r}'} \rho'\, d\rho'\, d\theta' \quad (14)$$

because the vector $\bar{p}$ is located in the $x-y$ plane. The Fourier inversion of (14) gives

$$\begin{aligned} \int \Delta\epsilon_r(\rho', \theta', z')\, dz' &= \frac{1}{4\pi^2} \iint \frac{1}{jk} \Gamma(p, \theta) e^{j\bar{p}\cdot\bar{r}'} p\, dp\, d\theta \\ &= C \iint \frac{1}{jp} \Gamma(p, \theta) e^{jp\rho'\cos(\theta - \theta' - \alpha/2)} p\, dp\, d\theta \\ &= C \iiint \frac{1}{jp} \Gamma(p, \theta) e^{jp\xi} \cdot \delta\left[\xi - \rho'\cos\left(\theta - \theta' - \frac{\alpha}{2}\right)\right] d\xi\, p\, dp\, d\theta \\ &= C \int \left[\int \left[\int \frac{1}{jp} \Gamma_\theta(p) e^{jp\xi} p\, dp\right] \cdot \delta\left[\xi - \rho'\cos\left(\theta - \theta' - \frac{\alpha}{2}\right)\right] d\xi\right] d\theta \end{aligned} \quad (15)$$

where $\Gamma_\theta(p)$ represents a p-space data line collected at a given θ direction, $C=\cos(\alpha/2)/2\pi^2$ is a constant depending on the bistatic angle, and ξ is the projected distance of position vector $\bar{r}'$ to the $\bar{p}$ vector at the $x-y$ plane. Recalling the spatial differentiation property of Fourier transformation, (15) can be rewritten as

$$\frac{\partial}{\partial\rho'}\int\Delta\epsilon_r(\rho',\theta',z')\,dz'=C\int\left[\int\left[\int\Gamma_\theta(p)e^{jp\xi}p\,dp\right]\cdot\delta\left[\xi-\rho'\cos\left(\theta-\theta'-\frac{\alpha}{2}\right)\right]d\xi\right]d\theta. \quad (16)$$

The left side in this equation represents the discontinuity in the $\vec{p}$ direction of the dielectric constant profile projected on the $x-y$ plane. The absolute value of the left side of (16) is defined as the dielectric image in this paper. This is based on the observation that an image is formed by reflection from interfaces or discontinuities. However, (16) indicates that the projection on the $x-y$ plane (z' integral) of the dielectric constant profile can be reconstructed from the accessed $\Gamma(p,\theta)/jp$ data, which is an inverse scattering problem.

The inner integral in (16) is a one-dimensional Fourier transform of a product of two terms, the first of which is a line of $\Gamma(p,\theta)$ in a fixed θ direction, and the second a ramp filter or Ramachandran–Lakshmanarayanan filter function [6]. This operation gives the projection data for each view angle or the range profile of the object which is the backscattered echo from the object when it is swept by a propagative impulse plane wave. The second integral is a back-protection operator for fixed angle θ. The outer integral is a θ summation of the back-projection data. This expression in (16) describes a filtered-back-projection algorithm [4] which is well known in CAT (computer-aided tomography). Note, in practice, $\Gamma_\theta(p)$ is only available over a certain spectral window [p_1 to p_2]. As a result, the reconstructed image is diffraction limited and is then an approximation of the true dielectric constant difference. The Fourier space data $\Gamma(p,\theta)$ can also be interpolated into a Cartesian format $\Gamma(p_x,p_y)$. Therefore a two-dimensional direct Fourier inversion of $\Gamma(p_x,p_y)$ would reconstruct the same dielectric image based on the projection-slice theorem.

Before proceeding to describe the experimental aspect of this work, a few remarks are made here to emphasize the distinction between the technique of X-ray tomography and this frequency-swept microwave tomographic imaging system. First, the data acquisition algorithm and the measurement instruments are different. X-ray tomography is an incoherent system which records the spatial-domain projections of the X-ray absorptivity of the test object on the viewing aperture. The described microwave imaging system is a coherent system that accesses the Fourier space of a scatterer by measuring the frequency response of the body as a function of aspect angle. The spatial-domain projections calculated from Fourier inversion give the derivative of the projected dielectric constant profile of the test object. A second distinction is that in X-ray tomography the line integral (or projection) is taken along the direction in which the X-ray radiation is beamed. In a microwave imaging system employing plane wave illumination, however, the integration is normal to the $\bar{p}$-line direction determined by the T/R positions. Therefore, the reconstructed image is derived from range information measured by each receiver, and the cross-range information is then obtained by processing many range returns observed in different scattering directions.

III. Experimental Results

In the following experiment, results of imaging a dielectric object consisting of two concentric plexiglass cylinders with top and bottom plexiglass lids situated in an anechoic chamber environment as shown in Fig. 3 are presented. The radii of the inner and outer cylinders are 4.7 cm and 15.0 cm, respectively. The lengths of the cylinders are 24.0 cm and the plexiglass walls are 0.3 cm thick. An HP8410B automated network analyzer is augmented to make multi-aspect scattered field measurements over a wide frequency band covering the 6–17 GHz range as described elsewhere [3]. The object is located about 8 m from the T/R antennas to satisfy the far-field criterion given in (11). For example if $r'=15$ cm and $f=17$ GHz, the right side of (11) becomes 4 m, which is less than the object range. A long metallic cylinder is used as the calibration object for system response characterization and range-phase term removal as described in [3].

A 2-D slice of the Fourier space data is formed by rotating the test object in azimuthal θ direction and measuring $\Gamma_\theta(p)$ for each rotation angle θ. In the measurement, two slices of the Fourier space data $\Gamma(p)$, shown in Fig. 4(a) and (b), are recorded for two elevation angles of the cylinders 0° and 90°, respectively. The data recording format used consisted of 256 radial lines covering an angular aperture of 360° with each line containing 64 frequency points. For the bistatic angle $\alpha=20°$ and the frequency range 6–17 GHz used in the recording geometry, the vector $\bar{p}=k(\hat{i}_r-\hat{i}_k)=2k\cos(\alpha/2)\hat{i}_p$ extends from $p_1=2.475$ rad/cm to $p_2=7.013$ rad/cm. The resulting range resolution is $\delta R=C/2\,\Delta f=2\pi/(p_2-p_1)=1.38$ cm, where Δf is the spectral range utilized.

Projection images of the plexiglass cylinders can then be reconstructed by applying either direct 2-D Fourier inversion or the filtered-back-projection algorithm to the accessed Fourier slice data. The 2-D inverse FFT of the $\Gamma(\bar{p})$ data requires its conversion first from the polar format in which it is originally acquired to a Cartesian format. This was achieved by means of a weighted average of the four nearest neighboring data points algorithm [7]. The interpolated Cartesian samples contain 128×128 samples over the region $p_x=(-7.01\sim7.01)$ rad/cm and $p_y=(-7.01\sim7.01)$ rad/cm, with the unavailable samples set to zero. A 2-D inverse FFT is then employed and the reconstructed images shown on the left side of Fig. 5 were obtained. The reconstructed images obtained by the filtered-back-projection operation are shown on the right

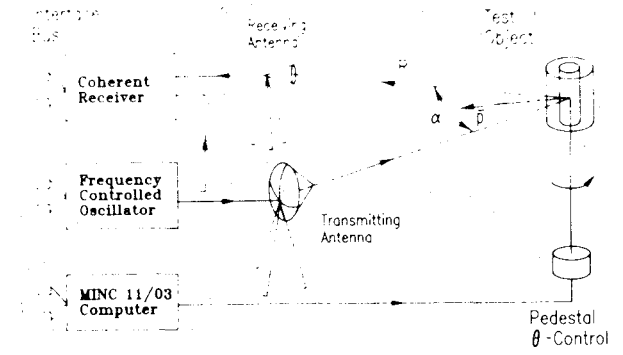

Fig. 3. Measurement arrangement in an anechoic chamber environment.

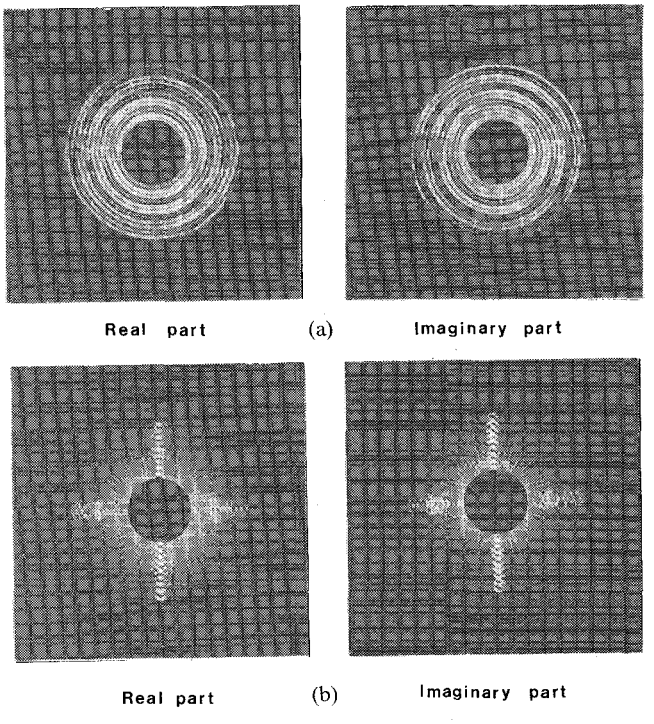

Fig. 4. Real part (left side) and imaginary part (right side) of accessed Fourier space data $\Gamma(\bar{p})$ of test object oriented at elevation angles (a) 0° and (b) 90°.

side of Fig. 5. A nearest four neighbors interpolation algorithm is used to transform the final back-projected image from a polar format to a Cartesian format for comparison.

The retrieved image for each elevation angle represents the projection of the scattering centers, such as walls and edges of the two cylinders, on the $x-y$ plane. The results shown in Fig. 5 bear close resemblance to the top view of the two cylinders for the two elevation angles 0° and 90°. Since the thickness of the plexiglass cylinder is less than the range resolution of the system, the front and back air–dielectric interfaces of the walls of the plexiglass cylinders are not resolved spatially and therefore are not differentiated in the reconstructed images.

In Fig. 5(b), where the test object is tilted 90° in elevation, the two bright horizontal lines represent the

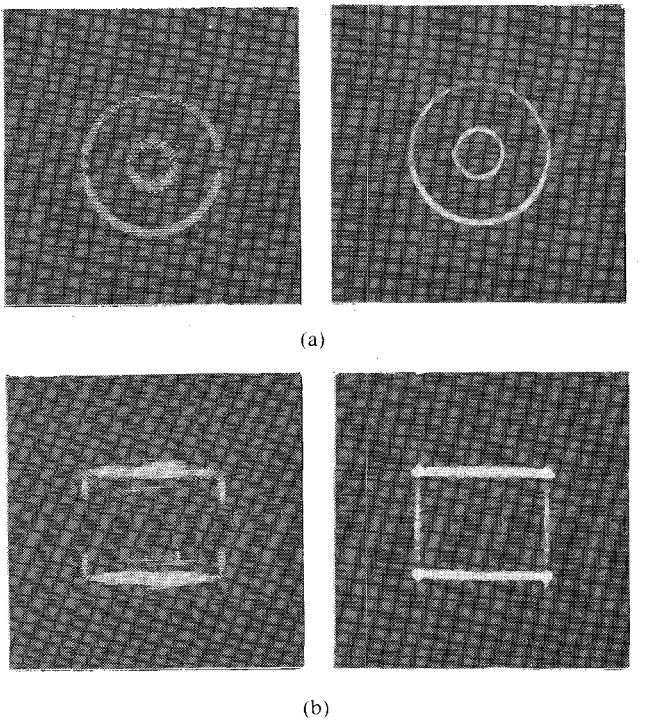

Fig. 5. Reconstructed dielectric images using direct Fourier inversion (left side) and filtered-back-projection algorithm (right side) of data shown in Fig. 4(a) and (b).

images of the top and bottom plexiglass lids, where strong specular reflections occur at certain values of θ. The images of the vertical lines contributed from the specular reflections from the walls of the two cylinders are dimmer due to the weaker specular reflection from the walls.

In the case considered here, the filtered-back-projection algorithm is seen to provide slightly better image quality than the direct Fourier inversion, because the two-dimensional inverse FFT requires both interpolation of the data $\Gamma(\bar{p})$ measured originally in polar samples to Cartesian samples and zero-padding in the unavailable region of Fourier space. However, in terms of computation time, the direct 2-D Fourier inversion is faster than the filtered-back-projection algorithm. A detailed study of Fourier inversion versus filtered back-projection methods as applied to dielectric imaging is found in [8].

IV. Conclusions

Both theoretical and experimental studies of microwave imaging of simple dielectric bodies under the first-order Born approximation have been discussed in this paper. The retrieved images shown are nearly free of the speckle noise that plagues conventional coherent imaging systems and particularly microwave imaging systems. Speckle noise suppression is attributed to the enhanced resolution of the wavelength diversity imaging technique.

The ability to image detail of the inner cylinder is evidence of the potential of microwave techniques using frequency and angular diversity in the imaging of internal structure and hence in nondestructive evaluation.

REFERENCES

[1] C. K. Chan and N. H. Farhat, "Frequency swept imaging of three-dimensional perfectly reflected objects," *IEEE Trans. Antennas Propagat.*, vol. AP-29, no. 2, pp. 312–319, Mar. 1981.

[2] N. H. Farhat, T. H. Chu, and C. L. Werner, "Tomographic and projective reconstruction of 3-D image detail in inverse scattering," *Proc. SPIE*, vol. 422, pp. 82–88, 1983.

[3] N. H. Farhat, C. L. Werner, and T. H. Chu, "Prospects for three-dimensional projective and tomographic imaging radar network," *Rad. Sci.*, vol. 19, no. 5, pp. 1347–1355, Sept. 1984.

[4] G. T. Herman, Ed., *Image Reconstruction from Projection Implementation and Application*. New York: Springer-Verlag, 1979.

[5] E. Wolf, "Three-dimensional structure determination of semitransparent objects from holographic data," *Opt. Commun.*, vol. 1, no. 4, pp. 153–156, 1969.

[6] G. N. Ramachandran and A. V. Lakshmanarayanan, "Three-dimensional reconstruction from radiographic and electron micrographic application of convolutions instead of Fourier transforms," *Proc. Nat. Acad. Sci. U.S.*, vol. 68, pp. 2236–2240, 1970.

[7] R. M. Mersereau and A. V. Oppenheim, "Digital reconstruction of multi-dimensional signals from their projections," *Proc. IEEE*, vol. 62, pp. 1319–1338, Oct. 1974.

[8] K. I. Schultz, "Reconstruction algorithms in microwave diffraction imaging," M.Sc. thesis, University of Pennsylvania, 1985.

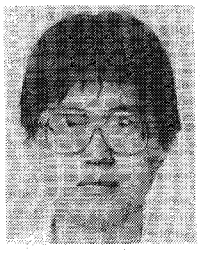

Tah-Hsiung Chu (M'87) was born in Taiwan on July 30, 1953. He received the B.S. degree from the National Taiwan University, Taipei, Taiwan, in 1976 and the M.S. and Ph.D. degrees from the University of Pennsylvania in 1980 and 1983 respectively, all in electrical engineering.

From 1983 to 1986 he was a member of the technical staff in the Microwave Technology Center at the RCA David Sarnoff Research Center in Princeton. Since 1986 he has been a Visiting Associate Professor with the Department of Electrical Engineering at the National Taiwan University. His research interests include microwave imaging system, microwave circuit and subsystem design, and digital and optical signal processing.

Nabil H. Farhat (S'58–M'63–SM'72–F'81) received the B.Sc. degree in 1957 from the Technion-Israel Institute of Technology, Haifa; the M.Sc. degree in 1959 from the University of Tennessee, Knoxville; and the Ph.D. degree in 1963 from the University of Pennsylvania, all in electrical engineering.

In 1964 he joined the faculty of the Moore School of Electrical Engineering, University of Pennsylvania, where he is now Professor in Electrical Engineering and heads the Electro-Optics and Microwave-Optics Laboratory. His current research interests are in image understanding, microwave imaging and holography, optical information processing and modeling of neural network and self-organizing systems, in all of which he has numerous publications. He teaches courses in EM theory, electro-optics and holography on both graduate and undergraduate levels. His past research included the study of the interaction of EM radiation with plasmas and solids in the context of laser output energy measurement and photodetachment of negative ions.

While Associate Professor, Dr. Farhat was named to the Ennis Chair in Electrical Engineering. In 1985 he was named Distinguished Visiting Scientist at the Jet Propulsion Laboratory in Pasadena. He is a recipient of the University of Pennsylvania Christian R. and Mary F. Lindback Foundation award for distinguished teaching. He is a Fellow of the Optical Society of America and a member of Sigma Xi, Eta Kappa Nu, the New York Academy of Science, the American Institute of Physics, the American Society for the Advancement of Science, and the Franklin Institute. He has served on the National Board of Directors of Eta Kappa Nu and has been an RCA consultant since 1969. Dr. Farhat has served as Editor of *Advances in Holography* and Associate Editor of *Acoustical Imaging and Holography*. He is currently engaged in the preparation of two texts: *An Introduction to Electro-Optics* and *Microwave Imaging* and *Holography-Theory and Applications*.